Originally published as:

Vieira Flauzino, J. V., Prado, T. L., Marwan, N., Kurths, J., Lopes, S. R. (2025): Quantifying Disorder in Data. - Physical Review Letters, 135, 9, 097401.

DOI: https://doi.org/10.1103/1y98-x33s

Quantifying disorder in data

João Vitor Vieira Flauzino,[1,2,3,4] Thiago Lima Prado,[1,4] Norbert Marwan,[3,5,6] Jürgen Kurths,[2,3,*] and Sergio Roberto Lopes[1,4,†]

[1]*Department of Physics, Federal University of Paraná,815 31-980, Curitiba, Brazil*
[2]*Department of Physics, Humboldt University Berlin, 12489 Berlin, Germany*
[3]*Potsdam Institute for Climate Impact Research (PIK), Member of the Leibniz Association, 14473 Potsdam, Germany*
[4]*Interdisciplinary Center for Science, Technology and Innovation CICTI, Federal University of Paraná,815 31-980, Curitiba, Brazil*
[5]*Institute for Physics and Astronomy, University of Potsdam, Potsdam, 14476, Germany*
[6]*Institute for Geosciences, University of Potsdam, Potsdam, 14476, Germany*

The quantification of disorder in data remains a fundamental challenge in science, as many phenomena yield short length datasets with order-disorder behavior, significant (un)correlated fluctuations, and indistinguishable characteristics even when arising from distinct natures, such as chaotic or stochastic processes. In this letter, we propose a novel method to directly quantify disorder in data through recurrence microstate analysis, showing that maximizing this measure is essential for its optimal estimation. Our approach reveals that the disorder condition corresponds to the action of the symmetric group on recurrence space, producing classes of equiprobable recurrence microstates. By leveraging information entropy, we define a robust quantifier that reliably differentiates between chaotic, correlated, and uncorrelated stochastic signals even using just small time series. Additionally, it uncovers the characteristics of corrupting noise in dynamical systems. As an application, we show that disorder minima over time often align with well-known stage transitions of the Cenozoic era, indicating periods of dominant drivers in paleoclimatic data.

The most important source of information about physical phenomena is the available data from them. Frequently, data comes from systems characterized by an interplay between order and disorder [1], posing an essential yet often overlooked question to understand the dynamics [2]. This problem becomes more challenging due to the finite size of the data and the presence of noise from experimental sources. Furthermore, even the fluctuations themselves may reveal physical properties [3, 4], mainly in cases of time-correlated stochasticity. In this sense, it is fundamentally important to acquire disorder-related characteristics of data across deterministic and stochastic contexts [5–8].

Complexity measures have been proposed to directly address data from phenomena involving disordered behavior [9–14], particularly with the goal of distinguishing between types of deterministic chaos and time-correlated or uncorrelated stochastic signals. These methods are often based on information entropy [15, 16] and serve as tools for quantifying disordered data [14, 17–21]. They typically involve encoding the time series into a set of symbols or partitions, with a corresponding probability distribution, to estimate complexity.

Unfortunately, these methods lack a general theoretical framework capable of explaining and classifying all the aforementioned contexts, which is even more problematic for higher-dimensional data and small size data [12, 22, 23]. In addition, many disorder-related quantifiers are sensitive to free-parameter choices tied to their computational methods. Although criteria for selecting parameters that yield appropriate partitions have been proposed, they are mainly established on heuristic ideas rather than formal, physically based reasoning [22, 24]. Also, such methods do not explicitly measure disorder, being influenced by other properties associated to the data complexity.

In this letter, we propose a recurrence-based method to quantify disorder in any kind of numerical data and show that the entropy maximization is a necessary strategy to acquire the optimal prediction of this property, eliminating free parameters. The method can thus distinguish between determinism, time-correlated and non-time-correlated-stochasticity by the disorder level of the data, and also identify the underlying characteristics of noise corrupting a system. Finally, we demonstrate the utility of the method in indicating transitions in Earth's paleoclimate dynamics via real-world data [25].

An ideal disorder condition implies classes of equiprobable matrices encoded from data, and the mean of the information entropy of these classes defines a disorder quantifier that increases as the condition is met. We refer to this quantifier as the Disorder Index via Symmetry in Recurrence Microstates (DISREM). To show this, let $\mathfrak{D} = (\mathbf{x}_i)_{i=1}^{K}$ be a tuple, namely a sequential representation of data elements. Inside $\mathfrak{D}$, there are smaller sequences $\mathbf{X}_{(n)}$ of N elements for $0 \leq n \leq K - N$ such that $\mathbf{X}_{(n)} = (\mathbf{x}_i)_{i=n+1}^{n+N}$.

(i) A description of disorder: The idea of completely disordered data means that it is dense and any event $\mathbf{X}_{(n)}$ must be entirely independent of all others [26]. To formalize this, we define an element $\tilde{\mathbf{x}}_i$ similar to $\mathbf{x}_i$ as $\tilde{\mathbf{x}}_i \in \{\mathbf{x} \in \mathfrak{D} : \|\mathbf{x}_i - \mathbf{x}\| < \delta\}$, in which δ is an arbitrary nonzero element. As $\delta \to 0$, the closer $\tilde{\mathbf{x}}_i$ is to $\mathbf{x}_i$. Then, the disorder density condition implies that there are other

data elements $\mathbf{x}_j$ corresponding to $\tilde{\mathbf{x}}_i$. Analogously, a subsequence similar to $\mathbf{X}_{(n)}$ is $\tilde{\mathbf{X}}_{(n)} = (\tilde{\mathbf{x}}_i)_{i=n+1}^{n+N}$. Since the disorder condition implies independence of all elements of $\mathbf{X}_{(n)}$, its probability of occurrence $p(\tilde{\mathbf{X}}_{(n)})$ is

$$p\left(\tilde{\mathbf{X}}_{(n)}\right) \equiv \prod_{i=n+1}^{n+N} p(\tilde{\mathbf{x}}_i). \tag{1}$$

(ii) Disorder condition through permutations: Eq. 1 implies that any permutation of the subsequence $\tilde{\mathbf{X}}_{(n)}$ has the same probability. Let σ be a permutation and S_N be the set of all possible permutations of N elements, so that $\sigma \in S_N$. The set S_N is the so-called symmetric group. Then, a direct consequence of Eq. 1 is:

$$p\left(\tilde{\mathbf{X}}_{(n)}\right) = p\left(\sigma(\tilde{\mathbf{X}}_{(n)})\right), \; \forall\, \sigma \in S_N. \tag{2}$$

(iii) Definition and properties of recurrence microstates: To define similar events or subsequences, avoiding the problem of selecting suitable partitions restricted to low-dimensional data [12, 22, 23], we analyze the data by using recurrences defined as $r_{(i,j)} = \Theta(\varepsilon - \|\mathbf{x}_i - \mathbf{x}_j\|)$, with Θ being the Heaviside function and ε the recurrence threshold. This procedure generates the matrix $\mathbf{M} \equiv \mathbf{R}(\mathbf{X}_{(n)}, \mathbf{X}_{(m)})$, where

$$\mathbf{R}(\mathbf{X}_{(n)}, \mathbf{X}_{(m)}) \stackrel{\text{def}}{=} \begin{bmatrix} r_{(n+1,m+1)} & \cdots & r_{(n+1,m+N)} \\ \vdots & \ddots & \vdots \\ r_{(n+N,m+1)} & \cdots & r_{(n+N,m+N)} \end{bmatrix}. \tag{3}$$

This square matrix for the case $N \ll K$ is called recurrence microstate of size N [17, 27] and consists of parts of the well-known recurrence plot defined as $\mathbf{R}(\mathfrak{D}, \mathfrak{D})$ [28]. This definition enables us to obtain self-relationships among the data based on a parameter ε, by comparing its elements directly and avoiding any reliance on partitioning via arbitrary segmentation of phase space.

When the size of the data K is increased, the probability of finding $\mathbf{x}_j$ progressively closer to another $\mathbf{x}_i$ increases as well. In these cases, the condition $\delta \ll \varepsilon$ is verified and for $K \to \infty$ even $\delta \to 0$ will satisfy $\mathbf{x}_i$ similar to $\mathbf{x}_j$. So we have

$$\mathbf{R}(\tilde{\mathbf{X}}_{(n)}, \tilde{\mathbf{X}}_{(m)}) \equiv \mathbf{R}(\mathbf{X}_{(n)}, \mathbf{X}_{(m)}). \tag{4}$$

The procedure for computing recurrence microstates involves counting the matrix generated by using $\tilde{\mathbf{X}}_{(n)}$ and $\tilde{\mathbf{X}}_{(m)}$ as inputs, but it also includes counting the reverse configuration. This implies that the probability of a microstate has the following property:

$$p\left(\mathbf{R}\left(\tilde{\mathbf{X}}_{(n)}, \tilde{\mathbf{X}}_{(m)}\right)\right) = p\left(\mathbf{R}\left(\tilde{\mathbf{X}}_{(m)}, \tilde{\mathbf{X}}_{(n)}\right)\right). \tag{5}$$

(iv) Consequence of disorder condition in recurrence microstates: Let σ_i and σ_j be permutations, $\sigma_i, \sigma_j \in S_N$. Then, Eq. 2 implies:

$$p\left(\mathbf{R}\left(\tilde{\mathbf{X}}_{(n)}, \tilde{\mathbf{X}}_{(m)}\right)\right) = p\left(\mathbf{R}\left(\sigma_i(\tilde{\mathbf{X}}_{(n)}), \sigma_j(\tilde{\mathbf{X}}_{(m)})\right)\right), \quad \forall\, \sigma_i, \sigma_j \in S_N. \tag{6}$$

(v) Consequences of permuting subsequences in recurrence microstates: To express the Eq. 6 in a matrix form, let $\mathcal{T}$ be the transposition operator of a matrix and $\mathcal{L}_\sigma$ be the operator that swaps rows as described by a given permutation σ. E.g., for $\sigma = 132$, the operator $\mathcal{L}_{132}$ swaps the third line by the second when applied to a matrix $\mathbf{M}$ of order $N = 3$, keeping the first line unchanged. Due to the definition 3 and Eq. 4, $\mathbf{M} \equiv \mathbf{R}(\tilde{\mathbf{X}}_{(n)}, \tilde{\mathbf{X}}_{(m)})$, then $\mathcal{L}_\sigma \mathbf{M} = \mathbf{R}(\sigma(\tilde{\mathbf{X}}_{(n)}), \tilde{\mathbf{X}}_{(m)})$ and $\mathcal{T}\mathbf{M} = \mathbf{R}(\tilde{\mathbf{X}}_{(m)}, \tilde{\mathbf{X}}_{(n)})$. It implies that:

$$\begin{cases} \mathbf{R}\left(\sigma_i(\tilde{\mathbf{X}}_{(n)}), \sigma_j(\tilde{\mathbf{X}}_{(m)})\right) = \mathcal{T}\mathcal{L}_{\sigma_j}\mathcal{T}\mathcal{L}_{\sigma_i}\mathbf{M} \\ \mathbf{R}\left(\sigma_j(\tilde{\mathbf{X}}_{(m)}), \sigma_i(\tilde{\mathbf{X}}_{(n)})\right) = \mathcal{L}_{\sigma_j}\mathcal{T}\mathcal{L}_{\sigma_i}\mathbf{M} \end{cases}. \tag{7}$$

(vi) Disorder condition implies classes of equiprobable microstates: Considering Eqs. 7 and 5, we rewrite Eq. 6 as $p(\mathbf{M}) = p(\mathcal{T}\mathcal{L}_{\sigma_j}\mathcal{T}\mathcal{L}_{\sigma_i}\mathbf{M}) = p(\mathcal{L}_{\sigma_j}\mathcal{T}\mathcal{L}_{\sigma_i}\mathbf{M})$, with $\sigma_i, \sigma_j \in S_N$. We now define the set of matrices generated by transpositions and all possible row swaps $\mathbf{M}$:

$$\mathscr{M}_a(\mathbf{M}) = \bigcup_{\sigma_i, \sigma_j \in S_N} \{\mathcal{L}_{\sigma_j}\mathcal{T}\mathcal{L}_{\sigma_i}\mathbf{M}, \quad \mathcal{T}\mathcal{L}_{\sigma_j}\mathcal{T}\mathcal{L}_{\sigma_i}\mathbf{M}\}. \tag{8}$$

We call $\mathscr{M}_a(\mathbf{M})$ the class of the microstate $\mathbf{M}$ generated by the disorder condition. Since the set of operations in Eq. 8 is induced by a group, any composition of operations is included in this set, ensuring the completeness of the disorder condition's implications. Then Eq. 6 becomes:

$$p(\mathbf{M}) = p(\mathbf{M}'), \; \forall\, \mathbf{M}' \in \mathscr{M}_a(\mathbf{M}). \tag{9}$$

(vii) A direct measure of disorder condition: Due to the finite data size and numerical errors in probability estimation, the probabilities of matrices in a class $\mathscr{M}_a$ will fluctuate around a constant value. This uniform distribution of microstate probabilities, as shown in Eq. 9, can be evaluated via information entropy: the smaller the fluctuations, the closer the probability distribution is to uniform, and the greater the resulting entropy.

Therefore, the recurrence threshold ε must be optimized to ensure a more accurate estimation of disorder. In contrast, the size of the microstate, N, is a descriptive parameter that allows us to compute disorder at a specified time scale. This means N is not a free parameter subject to optimization, as it is chosen to reflect the time scale of interest for measuring disorder.

We now define a function to quantify how much the data satisfies the disorder condition of Eq. 1. We look for a function Ξ, such that $0 \leq \Xi \leq 1$, that increases monotonically with the level of disorder, so that the maximum value of Ξ matches with the total disorder when the equiprobability predicted by Eq. 9 is perfectly satisfied.

If we compute the number of occurrences $\Omega(\mathbf{M})$ of a microstate $\mathbf{M} \in \mathscr{M}_a$, the total number of occurrences of the microstates belonging to the same class is $\sum_{\mathbf{M}' \in \mathscr{M}_a} \Omega(\mathbf{M}')$. Then, for each class $\mathscr{M}_a$, the probability of a microstate $\mathbf{M}$ is

$$p(\mathbf{M}) \equiv \frac{\Omega(\mathbf{M})}{\sum_{\mathbf{M}' \in \mathscr{M}_a} \Omega(\mathbf{M}')}. \tag{10}$$

Then, the information entropy $\xi_a(\varepsilon)$ associated with the probability distribution of microstates belonging to the same class $\mathscr{M}_a$ is

$$\xi_a(\varepsilon) \stackrel{\text{def}}{=} -\sum_{\mathbf{M} \in \mathscr{M}_a} p(\mathbf{M}) \ln p(\mathbf{M}). \tag{11}$$

Letting m_a be the number of matrices in the class of equiprobable microstates $\mathscr{M}_a$, then $\xi_a(\varepsilon) \to \ln m_a$. There is a finite number A of contributing classes to a given order N. Only two of these classes have just one microstate: the class of the microstate full of 0's and the class of the microstate full of 1's. It implies that the entropies of these classes are identically zero and they do not contribute to the number A. In this sense, $\xi(\varepsilon)$ is the total entropy of all classes computed summing up the entropy of each class and normalizing by its maximum possible amplitude A:

$$\xi(\varepsilon) \stackrel{\text{def}}{=} \frac{1}{A} \sum_{a=1}^{A} \frac{\xi_a(\varepsilon)}{\ln m_a}. \tag{12}$$

Finally, the normalized information entropy $\xi(\varepsilon)$ also monotonically increases with the disorder condition. As the disorder condition is increasingly satisfied, $\xi(\varepsilon) \to 1$. Theoretically, this occurs regardless of the parameter ε. But to measure disorder with the minimum error associated with the probability estimate, we must take the DISREM to be

$$\Xi = \max\left(\xi(\varepsilon)\right), \tag{13}$$

so that Ξ tends to 1 faster when the disorder condition is satisfied. This maximization is performed by testing a range of values ε at an adequate resolution. *In this case, the maximization of the entropy is a necessary strategy to the optimal computation of disorder.*

Models. We test the DISREM Ξ for six paradigmatic models [29]: (i) the logistic map, a chaotic system given by the equation $x_{t+1} = 4x_t(1 - x_t)$; (ii) white Gaussian noise (WGN), a normally distributed non-correlated stochastic signal; (iii) pink Gaussian noise (PGN) and (iv) red Gaussian noise (RGN), stochastic signals with a power spectrum distribution $P \propto 1/f^1$ and $P \propto 1/f^2$, respectively, generated using the Julia package `SignalAnalysis.jl` [29, 30]; (v) the autoregressive model (AR) generated by $\eta_t(\phi) = \phi\eta_{t-1} + w_t$, with $0 \le \phi < 1$ and w_t being white noise; (vi) noisy logistic map $y_t(\phi) = x_t + \eta_t(\phi)$, with a given variance ratio σ_η^2/σ_x^2, in which σ_x^2 and σ_η^2 are the variance of the logistic map x_t and AR-noise $\eta_t(\phi)$.

Validation. We perform all tests computing recurrence microstates of size $N = 4$ because this allows quantifying disorder on a sufficient time scale, avoiding higher computational costs of using $N > 4$. In the case of time series, there are $47,416$ possible recurrence microstates grouped into 147 classes, obtained by applying Eq. 8. Consequently, the number of possible classes contributing to the entropy is $A = 145$. Similarly, for $N = 3$ we have $A = 23$ and for $N = 2$, $A = 4$. The length K of the time series ranges from $10 \le K \le 10,000$.

We estimate Ξ for the noises WGN, PGN and RGN, as well as for the logistic map, by varying the time series length K (Fig. 1(a)). The WGN is the only signal that tends toward the maximum value, since it is a completely uncorrelated noise. Because RGN has stronger temporal correlation than PGN, its corresponding disorder value is lower. Furthermore, all stochastic signals display distinct disorder values compared to the chaotic deterministic behavior of the logistic map.

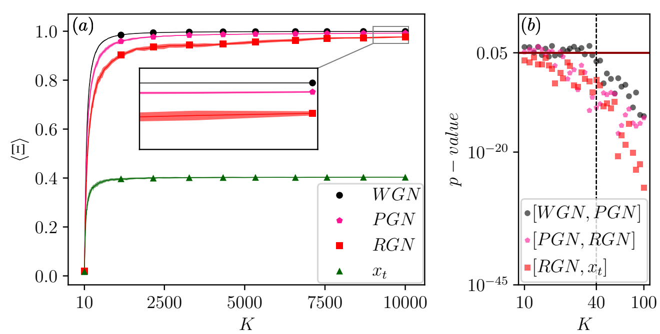

Figure 1. (a) The mean of the DISREM $\langle\Xi\rangle$, Eq. 13, as a function of the length of the time series K for the logistic map, WGN, PGN and RGN [29]. Since WGN is the only random uncorrelated process, the more data we have, the better the disorder tends to the maximum $\Xi = 1$. The correlated signals PGN and RGN do not satisfy the disorder condition, but they still reach values greater than the chaotic logistic map. We compute the quantifier over 30 time series for each model, at a timescale $N = 4$. (b) The p-values [31] of Welch's t-test $[p, q]$ comparing the mean of disorder for the model p and model q as a function of the time series length. For $K > 40$, all p-values are less than 0.05, indicating that the mean value of each curve in (a) is distinguishable.

The differences in the disorder values for the models are statistically significant, as tested with a Welch's t-test [31] (testing that the disorder values for models p and q come from distributions with equal means). For $K > 40$, all p-values are below 0.05, indicating that it is possible to distinguish the mean disorder values for the WGN, PGN, RGN and logistic map with more than 95% confidence when $K > 40$ (Fig. 1(b)).

For the autoregressive model, increasing the parameter ϕ enhances the dependence on past values of the process. Then, the disorder decreases as ϕ increases (Fig. 2).

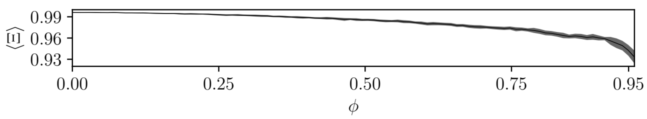

Figure 2. The mean of the DISREM $\langle\Xi\rangle$, Eq. 13, for the autoregressive model. The disorder decreases as the parameter ϕ increases, since ϕ defines the past dependence of the noise. DISREM computed over 30 time series of length 3,000, at a timescale $N = 4$.

We compute the DISREM to the noisy logistic map using AR-noise with $\phi = 0.00$, $\phi = 0.25$, $\phi = 0.50$, $\phi = 0.75$ and $\phi = 0.90$. Varying the variance ratio σ_η^2/σ_x^2, the data transitions from a purely deterministic signal ($\sigma_\eta^2/\sigma_x^2 = 0$) to a stochastic process ($\sigma_\eta^2/\sigma_x^2 = 1$). The DISREM increases as the noise variance $\sigma_\eta^2 \to \sigma_x^2$, but the rate of increase differs gradually depending on the value of the correlation parameter ϕ (Fig. 3(a)). Similarly, we find p-values lower than 0.05 to any variance ratio $\sigma_\eta^2/\sigma_x^2 > 0$ (Fig. 3(b)). These results imply that each curve in figure 3(a) is distinguishable from the closest other curve.

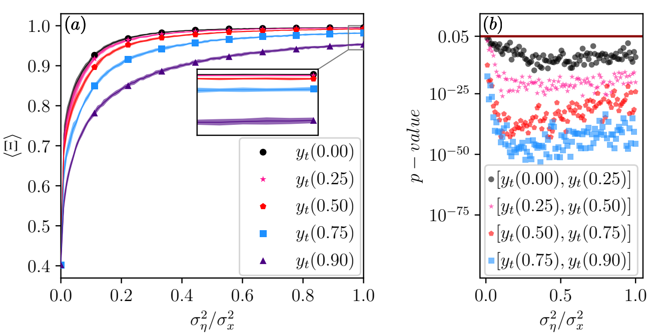

Figure 3. (a) The mean of the DISREM $\langle\Xi\rangle$, Eq. 13, for the noisy logistic model $y_t(\phi) = x_t + \eta_t(\phi)$ as a function of the ratio σ_η^2/σ_x^2 between the variance σ_η^2 of the noise $\eta_t(\phi)$ and the variance σ_x^2 of the logistic map x_t. The disorder increases as noise variance increases, but grows more slowly as the past dependence parameter ϕ of the noise increases. We compute the disorder over 30 time series of length 3000, at a timescale $N = 4$. (b) The p-values [31] of Welch's t-test $[p, q]$ comparing the mean of disorder for the model p and model q as a function of the variance ratio σ_η^2/σ_x^2. Each p-value is less than 0.05, indicating a statistically significant ability to distinguish the degree of correlation in the noise influencing a system.

Applications on real-world data. Finally, we investigate the temporal evolution of disorder in the palaeoclimate via the Cenozoic Global Reference benthic foraminifer carbon and oxygen isotope dataset (CENOGRID) [25]. These records archive long-term changes in Earth's carbon cycle, deep-sea temperature, and seawater composition, serving as a stratigraphic reference for global climate evolution over the past 66 million years, the Cenozoic era. Previous studies have indicated a decrease in its *predictability* over time. The DISREM supports this conclusion, showing a clear increase in disorder (Fig. 4). By comparing the mean disorder values from stochastic models, we observe that CENOGRID transitions from a disorder level similar to RGN to one resembling WGN.

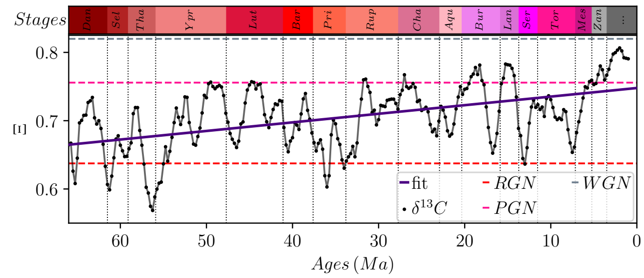

Figure 4. The DISREM Ξ, Eq. 13, for benthic foraminifer carbon isotope $\delta^{13}C$ data as a function of age in million years ago (Ma) [25]. Each value was calculated using a sliding window of length $K = 200 \equiv 2$ Ma and $N = 4 \equiv 0.04$ Ma. The background shows the mean disorder values for WGN, PGN, and RGN, computed with $K = 200$. A linear fit illustrates the overall increase in disorder over time. Vertical dotted lines indicate stage divisions, corresponding to minimum points in the disorder measure linked to the driving triggers of transitions. Dan, Danian; Sel, Selandian; Tha, Thanetian; Ypr, Ypresian; Lut, Lutetian; Bar, Bartonian; Pri, Priabonian; Rup, Rupelian; Cha, Chattian; Aqu, Aquitanian; Bur, Burdigalian; Lan, Langhian; Ser, Serravallian; Tor, Tortonian; Zan, Zanclean.

The stage transitions (Fig. 4) are associated with driving triggers like astronomical forcing and tectonic activity [32]. If a factor amplifies its influence while diminishing the impact of others, it can lead to a shift of stages. In terms of disorder, this dominance resembles the situation depicted in Fig. 3 where the variance of a primary trigger σ_x^2 increases relative to other factors (considered as noise with a variance σ_η^2), overall decreasing disorder. This is why disorder minima often align with stage transitions (Fig. 4), indicating periods of relative regularity of the carbon isotope $\delta^{13}C$ data under a dominant forcing. Significant events also reflect on disorder along stages, e.g. in the Eocene-Oligocene Transition in 34 million years ago (Ma), the decline of atmospheric carbon dioxide levels had a central role to the development of the Antarctic ice sheet [33] and corresponds to an average decrease in disorder during earlier stages.

Overall, we have applied the disorder condition, interpreted as full independence of past states, in the definition of recurrence microstates. This leads to an action of the symmetric group on the recurrence space and creates classes of equiprobable microstates. We propose a quantifier, DISREM, defined by the mean of information entropies of all classes, which increases as the disorder condition is met. We have demonstrated that maximizing this entropy-based quantifier is necessary for its optimal estimation, resulting in a parameter-free, direct measure of disorder in data, given a timescale. Statistical tests of the DISREM on deterministic and stochastic models demonstrate its ability to distinguish between chaotic, correlated, and uncorrelated signals using relatively short time series. The method can characterize the correlation level of corrupting noises in dynamical systems and outperforms other measures due to its sensitivity, interpretability, dimension-free computation, and self-tuning capability (see End Matter). Additionally, its application to experimental data from the Cenozoic era reflects the major climate transitions in Earth's system dynamics. Thus, the proposed quantifier is a useful tool for understanding the underlying nature of complex phenomena.

* juergen.kurths@pik-potsdam.de
† lopes@fisica.ufpr.br, Permanent address at Department of Physics, Federal University of Paraná.
[1] T. Shinbrot and F. J. Muzzio, Nature **410**, 251 (2001).
[2] D. Sornette, *Critical phenomena in natural sciences: chaos, fractals, selforganization and disorder: concepts and tools* (Springer Science & Business Media, 2006).
[3] S. Kos and P. Littlewood, Nature **431**, 29 (2004).
[4] S. A. Crooker, D. G. Rickel, A. V. Balatsky, and D. L. Smith, Nature **431**, 49 (2004).
[5] E. C. Barrows, in *Maximum Entropy and Bayesian Methods: Laramie, Wyoming, 1990* (Springer, 1991) pp. 191–197.
[6] N. Marwan and J. Kurths, Physica D **238**, 1711 (2009).
[7] C. Letellier, *Chaos in Nature* (World Scientific, 2013) https://www.worldscientific.com/doi/pdf/10.1142/8312.
[8] T. N. Palmer, Nature Reviews Physics **1**, 463 (2019).
[9] M. B. Kennel and S. Isabelle, Physical Review A **46**, 3111 (1992).
[10] D. T. Kaplan and L. Glass, Physical Review Letters **68**, 427 (1992).
[11] O. A. Rosso, H. Larrondo, M. T. Martin, A. Plastino, and M. A. Fuentes, Physical Review Letters **99**, 154102 (2007).
[12] A. Politi, Physical Review Letters **118**, 144101 (2017).
[13] D. Toker, F. T. Sommer, and M. D'Esposito, Communications Biology **3**, 11 (2020).
[14] T. L. Prado, B. R. R. Boaretto, G. Corso, G. Z. dos Santos Lima, J. Kurths, and S. R. Lopes, New Journal of Physics **24**, 033027 (2022).
[15] C. E. Shannon, Bell System Technical Journal **27**, 379 (1948).
[16] S. M. Pincus, Proceedings of the National Academy of Sciences **88**, 2297 (1991).
[17] G. Corso, T. L. Prado, G. Z. d. S. Lima, J. Kurths, and S. R. Lopes, Chaos **28**, 083108 (2018).
[18] X. Xu, J. Zhang, and M. Small, Proceedings of the National Academy of Sciences **105**, 19601 (2008).
[19] C. Bandt and B. Pompe, Physical Review Letters **88**, 174102 (2002).
[20] Y. Hirata, Communications in Nonlinear Science and Numerical Simulation **94**, 105552 (2021).
[21] Y. Hirata and J. Amigó, Chaos **33**, 052101 (2023).
[22] P. Grassberger and H. Kantz, Physics Letters A **113**, 235 (1985).
[23] F. Christiansen and A. Politi, Physica D **109**, 32 (1997).
[24] N. Marwan and K. H. Kraemer, The European Physical Journal Special Topics **232**, 5 (2023).
[25] T. Westerhold, N. Marwan, A. J. Drury, D. Liebrand, C. Agnini, E. Anagnostou, J. S. K. Barnet, S. M. Bohaty, D. D. Vleeschouwer, F. Florindo, T. Frederichs, D. A. Hodell, A. E. Holbourn, D. Kroon, V. Lauretano, K. Littler, L. J. Lourens, M. Lyle, H. Pälike, U. Röhl, J. Tian, R. H. Wilkens, P. A. Wilson, and J. C. Zachos, Science **369**, 1383 (2020).
[26] C. Letellier, I. Leyva, and I. Sendiña-Nadal, Physical Review E **101**, 022204 (2020).
[27] T. L. Prado, G. Z. dos Santos Lima, B. Lobão Soares, G. C. do Nascimento, G. Corso, J. Fontenele-Araujo, J. Kurths, and S. R. Lopes, Chaos **28**, 085703 (2018).
[28] N. Marwan, M. C. Romano, M. Thiel, and J. Kurths, Physics Reports **438**, 237 (2007).
[29] J. C. Sprott, *Chaos and Time-Series Analysis* (Oxford University Press, 2003).
[30] M. Chitre, Signalanalysis.jl (2024), gitHub repository. Available at: `https://github.com/org-arl/SignalAnalysis.jl` [Accessed: 2023-09-16].
[31] J. H. Zar, *Biostatistical Analysis*, 5th ed. (Prentice-Hall, 2009).
[32] R. Fortey, *Life: A Natural History of the First Four Billion Years of Life on Earth* (Vintage, 1999).
[33] P. N. Pearson, G. L. Foster, and B. S. Wade, Nature **461**, 1110 (2009).
[34] R. Zwanzig, Nonequilibrium Statistical Mechanics **3** (2001).
[35] C. Bandt and B. Pompe, Physical Review Letters **88**, 174102 (2002).
[36] S. He, K. Sun, and H. Wang, Physica A **461**, 812 (2016).
[37] R. L. Ruiz, H. Mancini, and X. Calbet, in *Concepts and Recent Advances in Generalized Information Measures and Statistics* (Bentham Science Publishers, 2013) pp. 147–168.
[38] G. Datseris and K. A. Haaga, arXiv preprint arXiv:2406.05011 (2024).
[39] G. Datseris, Journal of Open Source Software **3**, 598 (2018).

END MATTER

The objective of this section is to provide further examples and to compare the proposed approach with similar methods. We present tests for five additional models, all of which exhibit DISREM results comparable to those of the Logistic map and the types of noise discussed. For each model, we set the control parameter to p_2 to induce a well-known increase in disorder compared to its value at p_1. For each case, we computed 50 datasets of length $K = 3000$. To further test the method's robustness, continuous systems were undersampled at a timestep of 0.5, disregarding a transient time of 1000.0. The initial conditions for discrete systems were selected in the chaotic sea, while for the others, they were set randomly. Since multivariate data enables 65,536 recurrence microstates of size $N = 4$, applying Eq. 8 to all these matrices results in $A = 190$ contributing classes, compared to $A = 145$ for (univariate) time series. Consequently, the normalization factor A is automatically adjusted according to the dimensionality.

Models. (vii) Double-gyre system [26] defined as $\dot{x} = p_{1,2}\pi \sin\left[\pi(ux^2 + x - u)\right] \sin \pi y$, $\dot{y} = p_{1,2}\pi \cos\left[\pi(ux^2 + x - u)\right] \cos \pi y$, $\dot{u} = v$, $\dot{v} = -(\frac{\pi}{5})^2 u$, with parameter values $p_1 = 0.25$ and $p_2 = 0.10$. (viii) Lorenz system [29], $\dot{x} = 10(y-x)$, $\dot{y} = x(p_{1,2}-z)-y$, $\dot{z} = xy - \frac{8}{3}z$, with $p_1 = 24$ and $p_2 = 32$. (ix) Standard map [29], $\theta_{n+1} = (\theta_n + \rho_{n+1}) \mod 2\pi$, $\rho_{n+1} = \rho_n + p_{1,2}\sin\theta_n \mod 2\pi$, with $p_1 = 1.0$ and $p_2 = 2.0$. (x) The previously defined noisy logistic model, but with $\sigma_\eta^2/\sigma_x^2 = 0.3$, $\phi = p_1 = 0.50$ and $\phi = p_2 = 0.25$, hereafter refered to as GNL (Gaussian-noisy logistic). (xi) Langevin equation [34], $\frac{dv}{dt} = -p_{1,2}v + w_t$, with $p_1 = 0.1$ and $p_2 = 1.0$. Remember, w_t is white Gaussian noise. (xii) Time series [26] s_t of the logistic map $y_{t+1} = 3.99\, y_t(1 - y_t)$ with uniform white noise added u_t, such that $s_t = (1 - p_{1,2})y_t + p_{1,2}u_t$, where $p_1 = 0.45$ and $p_2 = 0.55$, referred to as UNL (uniform-noisy logistic).

DISREM, Ξ, consistently increases as the control parameter changes from p_1 to p_2 (Fig. 5). Furthermore, all disorder values for these paradigmatic stochastic cases exceed $\Xi = 0.94$, while the dynamical systems analyzed exhibit disorder values below $\Xi = 0.8$, despite data undersampling. These results confirm a significant difference between the disorder values of typical stochastic processes and deterministic systems and reinforce the robustness of Ξ in quantifying order-disorder phenomena.

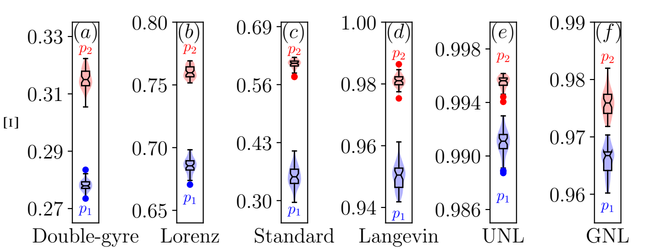

Figure 5. Boxplots with violin plots showing the values of the proposed quantifier, DISREM Ξ, for each model and its parameter values p_1 and p_2.

We conduct analyses on the same generated datasets, comparing DISREM with six well-known methods: permutation entropy (PE) [35], multivariate permutation entropy (MvPE) [36], statistical complexity (SC) [11, 37], determinism by recurrence quantification (DET) [**?**], structurality (Δ) [26] and dynamical complexity (DC) [26]. All methods were implemented using the Julia language packages `ComplexityMeasures.jl` [38] and `RecurrenceAnalysis.jl` [39], except for Δ and DC, implemented directly.

The DET quantifier is expected to increase toward 1 for more deterministic systems. For parameter selection, we set the recurrence threshold using the Julia function `GlobalRecurrenceRate(0.10)`, fixing a 10% recurrence rate [25]. In critical cases (Fig. 6), the Standard deterministic map exhibits high DET values (> 0.5), with the disorder-inducing parameter value p_2 reducing DET compared to p_1, as expected. However, the Lorenz model exhibits lower DET values for p_2, contradicting the expected behavior. Additionally, the Lorenz model yields DET values similar to those of correlated noises from the Langevin equation, blurring the distinction between signals of deterministic and stochastic nature.

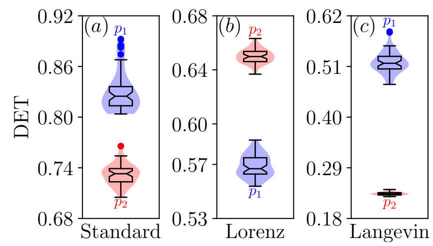

Figure 6. Boxplots with violin plots showing the values of the Determinism (DET) for critical cases.

Permutation entropy (PE) and multivariate permutation entropy (MvPE) are natural measures of complexity, increasing with system complexity. For PE, we set the ordinal pattern length to $m = 6$ and the embedding delay $\tau = 1$ [11], and for MvPE, m matches the data dimension. In critical cases (Fig. 7), the double-gyre system

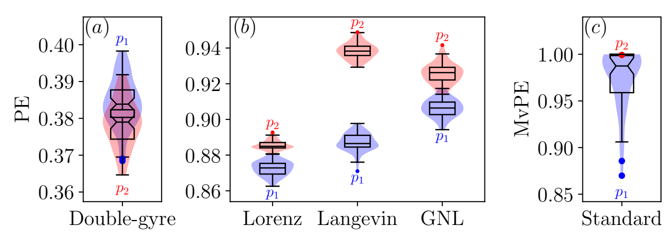

Figure 7. Boxplots with violin plots showing the values of the permutation entropy (PE) and multivariate permutation entropy (MvPE) for critical cases.

and the GNL show overlapping PE values for parameter values p_1 and p_2, making it difficult to detect the expected increase in disorder. Additionally, the deterministic Lorenz system shows PE values comparable to those of the stochastic Langevin equation. The MvPE

Quality	DISREM	DET	PE	MvPE	SC	Δ	DC
Correct and statistically significant distinction of disorder-inducing parameter values (p_1 and p_2) for all tested models	Yes	No	No	No	No	No	No
Correct distinction of deterministic and stochastic typical cases	Yes	No	No	No	Yes*	No	No
Independence of dimensionality	Yes	Yes	No	Yes	No	Yes	Yes
Optimal and inherent selection of its parameters	Yes	No	No	Yes	Yes	Yes	Yes
Direct interpretation via a single measure	Yes	Yes	Yes	Yes	No*	Yes	No

*: if used together with PE.

Table I. Summary of the comparison between the proposed DISREM and similar traditional methods.

value, in turn, unexpectedly reaches its maximum possible value for the standard map.

The statistical complexity (SC) typically decreases for white noise and increases for chaos, complementing permutation entropy (PE). Since SC depends on PE for its computation, its values are presented in the boxplots for critical cases, with the multivariate version referred to as MvSC. The results (Fig. 8) align with those from PE, though combining SC and PE in a plane could enhance the analysis. However, this approach makes data interpretation more indirect, complicating direct temporal analysis of disorder.

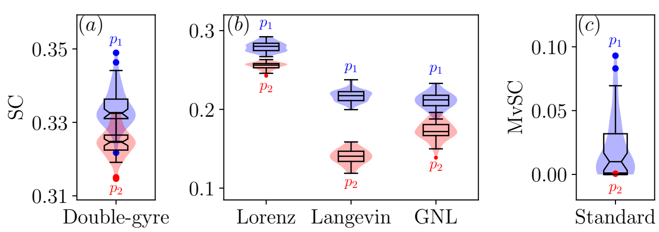

Figure 8. Boxplots with violin plots showing the values of the statistical complexity (SC) for critical cases.

The structurality (Δ) [26] is the fraction of visited boxes from a pixelation of the Poincaré section, such that a lack of describability in the structure of the dynamics manifests as a large Δ, while $\Delta \approx 0$ for well-ordered dynamics. Although it performs well in some scenarios (Fig.9(a)–(b)), showing agreement with the proposed quantifier (Fig.5(a),(c)), it yields overlapping values for the UNL and GNL (Fig.9(c)–(d)). The dynamical complexity (DC), a sum of Δ and PE, also succeeds with the standard map and yields overlapping values for the GNL (Fig. 9(e)). Both Δ and DC produce values for the GNL in the range of the standard map, indicating similar outcomes for deterministic and stochastic models.

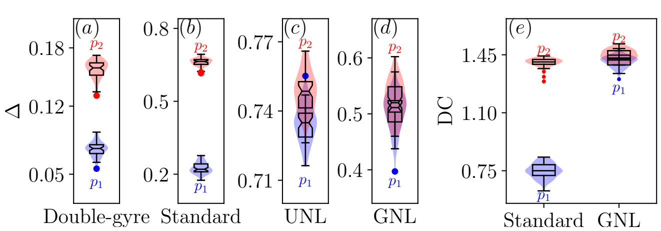

Figure 9. Boxplots with violin plots showing the values of the (a)-(d) structurality Δ and (e) dynamical complexity (DC) for critical cases.

In contrast, the DISREM Ξ outperforms other measures by remaining distinguishable across the tested parameter regimes and yielding higher values for typical stochastic cases than for deterministic dynamics (Fig. 5). The discussions are summarized in the table I, highlighting some advantages of the DISREM compared to each measure across the benchmark models. These results support the claim that the proposed quantifier is an optimal method for directly measuring the degree of disorder in any type of multivariate data, demonstrating robustness even when applied to short datasets with low temporal resolution while maintaining consistent performance, interpretability, and statistical significance.